Publ. Astron. Soc. Japan 30, 563-579 (1978)

Evolution of Supernova Remnants. I. Interacting Supernova Remnants

Satoru IKEUCHI

Department of Physics, Hokkaido University, Sapporo 060

(Received 1977 December 17; revised 1978 March 11 and 1978 April 8)

Abstract

The evolution and structure of two interacting supernova remnants (SNRs) are calculated by use of a time-dependent two-dimensional hydrodynamic code. The interactions of two SNRs are simulated in such a way that at a time t_0 after the first supernova explosion, the second supernova explosion occurs at the distance D and two SNRs encounter. Two cases are investigated; the second explosion occurs outside or inside the expanding shell of the first SNR. In the first case, the final structures of two interacting SNRs are typically classified into three types: (1) two SNRs merge into a single-like SNR, (2) two SNRs merge but show a peanut-shape structure, and (3) two SNRs do not merge. In the second case, they reduce to two types: (1) two SNRs evolve as an isolated SNR with twice the explosion energy, and (2) in the shell of the first SNR a bump is formed due to the shock impact by the second explosion. The critical distances for the above structural changes are examined, as well as the changes of the expansion law from an isolated SNR. With these results some discussions are given on the formation of an SNR tunnel system and the possibility of gas ejection from a galaxy. Based upon this view of interacting SNRs, a preliminary model for the solar neighborhood and loop I is presented.

Key words: Interstellar matter; Shock waves; Supernova remnants; X-rays.

1. *Introduction*

Observations of the diffuse component of soft X-rays (Burstein et al. 1977; Tanaka and Bleeker 1977) and the ultraviolet absorption spectrum (Spitzer and Jenkins 1975) indicate that hot components of temperatures higher than 10^5 K occupy a considerable volume of the interstellar space. These hot components have a large size and are preferentially located in the regions of H I minima.

On the origin of these hot components, two pictures are proposed, i.e., supernova remnants (SNRs) (Cox and Smith 1974; Smith 1977; Hayakawa et al. 1977) and hot bubbles formed by stellar wind (Castor et al. 1975). The hot components, which show X-ray emission features of temperatures higher than 10^6 K, seem to be attributed to SNRs. Besides the known SNRs such as the Cygnus loop, the Vela SNR, and the Puppis SNR, there are several X-ray enhancements which

may be candidates of SNRs, such as loop I (the North Polar Spur) (Burstein et al. 1977; Cruddace et al. 1976; Hayakawa et al. 1977; Borken and Iwan 1977), the region in constellation Eridanus (Naranan et al. 1976), and the Lupus region (Burstein et al. 1977; Hayakawa et al. 1975).

As for the spherical expansion of the SNR shell in a uniform medium, some analytical (Sedov 1959; Woltjer 1972) and numerical (Chevalier 1974; Mansfield and Salpeter 1974; Straka 1974) calculations have been made, and the evolution and structure of an isolated SNR have been fully clarified.

However, the observational features of SNRs do not always show a simple spherical shape. The first cause is that the ambient matter is not homogeneous, but usually inhomogeneous. The second cause of the non-sphericity of SNRs is the interactions of SNRs with each other. As is proposed by Cox and Smith (1974) and by Smith (1977), the intersections of SNRs and the formation of SNR-tunnel systems are expected in our Galaxy if the supernova explosion rate is greater than $1.5\times10^{-7}\,\mathrm{Myr}^{-1}\,\mathrm{pc}^{-3}$. Till now, we have no direct evidence for these SNR-chains, but some indications are pointed out in the Eridanus region and in the contact edge between the hot gas in the solar neighborhood and loop I (Tanaka and Bleeker 1977) and between loop I and loop IV (Borken and Iwan 1977). The third cause of the non-spherical SNR is the effect of the anisotropy of the compressed magnetic field. The most typical one is the Crab nebula, although this seems to be an exceptional SNR among others.

In the present and subsequent papers, the evolution and structure of SNRs for the cases of interacting SNRs (present paper), of SNR-cloud collision (paper II) and of large-scale expansion of an SNR in a plane-stratified medium (paper III) are studied. The effect of the magnetic field is not included in this series.

In the present paper, we investigate the evolution of two interacting SNRs in a uniform ambient medium. The purpose of this study is to make clear the following two problems: (1) How are the evolution (expansion law) and the structure (distribution of gas density) of interacting SNRs different from an isolated SNR? (2) What is the probability to form SNR-chains in our Galaxy, and what effects are brought about on the evolution and structure of a galaxy?

In section 2, basic equations and input data for numerical calculations are described, and the standard model of an isolated SNR is given. In sections 3 and 4, numerical results of interacting SNRs are presented for the second supernova explosions outside and inside the first SNR shell, respectively. In section 5, typical X-ray profiles are presented, bearing in mind the X-ray observations of two-interacting SNRs. In the final section, some discussions on the formations of SNR-chains are given.

2. *Basic Equations and Data for Numerical Calculations*

The evolution of a remnant after the point explosion of a supernova is calculated by use of the time dependent, two-dimensional hydrodynamic code of Eulerian scheme. The gas is assumed to be an ideal one with the adiabatic exponent $\gamma=5/3$ and to be under local thermal equilibrium.

2.1. *Basic Equations and Numerical Procedures*

In the cylindrical coordinates (r,θ,z), the conservation equations of mass, r-momentum, z-momentum, and internal energy are written as

$$\frac{\partial}{\partial t}\rho+\mathrm{div}\,(\rho\boldsymbol{v})=0\ , \tag{2.1}$$

$$\frac{\partial}{\partial t}(\rho u)+\mathrm{div}\,(\rho u\cdot\boldsymbol{v})=-\frac{\partial P}{\partial r}-g_r\rho\ , \tag{2.2}$$

$$\frac{\partial}{\partial t}(\rho v)+\mathrm{div}\,(\rho v\cdot\boldsymbol{v})=-\frac{\partial P}{\partial z}-g_z\rho\ , \tag{2.3}$$

and

$$\frac{\partial}{\partial t}(\rho\varepsilon)+\mathrm{div}\,(\rho\varepsilon\cdot\boldsymbol{v})=-P\,\mathrm{div}\,(\boldsymbol{v})+\Lambda\ , \tag{2.4}$$

where ρ, P, ε, and $\boldsymbol{v}=(u, 0, v)$ are the density, the pressure, the internal energy of unit mass, and the velocity. From the equation of state, we obtain $P=(\gamma-1)\rho\varepsilon=2\rho\varepsilon/3$ and the temperature $T=\mu HP/k\rho$, where μ, H, and k are the mean molecular weight, the mass of hydrogen atom, and the Boltzmann constant. The external gravity $\boldsymbol{g}=(g_r, 0, g_z)$ is neglected in the present computation. The rate of radiative cooling Λ is described in subsection 2.2.

For computational convenience, the physical quantities are normalized to mesh sizes Δr, Δz, and Δt as

$$r'=r/\Delta r\ ,\qquad z'=z/\Delta z\ ,\qquad t'=t/\Delta t\ ,\qquad \rho'=\rho/\rho_0\ , \tag{2.5}$$

where ρ_0 is the density of the ambient matter. Then, equations (2.1)–(2.4) are rewritten by normalized quantities when the velocity and the pressure are scaled by $(\Delta r/\Delta t)$ and $\rho_0(\Delta r/\Delta t)^2$, respectively. The volume of the explosion point V_0 is defined by $M_0=\rho_0 V_0$, where M_0 is the total ejected mass. The explosion energy is given by $E_0=M_0(\Delta r/\Delta t)^2/2$. We adopt E_0 and ρ_0 as 10^{51} erg and 1.7×10^{-24} g cm^{-3}, respectively, and the mesh size Δr $(=\Delta z)$ as 4.0 pc. In this case, the total ejected mass becomes $M_0=4.3M_\odot$. As the mesh size is rather large, the structure of the shocked shell can be calculated only as an averaged one. Numerical integrations have been performed by means of the Lax-Wendroff-type difference method to the second order (Lax 1954; Lax and Wendroff 1966). Shock waves are treated by utilizing truncation errors of the finite-difference equation.

In the calculation of interacting SNRs, the line connecting two-explosion points is chosen as the Z-axis, and the whole structure is assumed to be axially symmetric. This corresponds to a head-on collision in the case of the two-body encounter.

2.2. *Radiative Cooling*

Thermal bremsstrahlung is due practically to completely ionized H and He. If their mixing ratio is the same as that of their cosmic abundances, it gives the cooling rate as

$$\Lambda(\mathrm{brems})=1.59\times10^{-24}\bar{g}_B n^2 T_6^{1/2}\ \mathrm{erg\ cm^{-3}\ s^{-1}}\ , \tag{2.6}$$

where $\bar{g}_B$ is the average gaunt factor which is assumed to be unity, and n and T_6 are the number density of electrons and the temperature in units of 10^6 K.

In the range 10^4–10^6 K, line emission due to collisional excitation becomes important. The rate of radiation loss (Cox and Tucker 1969) is approximated as

$$\Lambda_c = 1.11\times10^{-20} n^2 T_6^{3/2} \qquad 10^3\,\mathrm{K} < T < 2\times10^5\,\mathrm{K}\,, \tag{2.7}$$

$$= 1.99\times10^{-22} n^2/T_6 \qquad 2\times10^5\,\mathrm{K} < T < 10^7\,\mathrm{K}\,, \tag{2.8}$$

for a mixture of elements of cosmic abundances. In reality, the coronal equilibrium assumed in Cox and Tucker (1969) is not satisfied in the SNR shell, as made clear by Itoh (1977) and Hayakawa et al. (1978). However, the dynamical features of SNR expansion will not change much from the results in this paper. The total loss rate is given as $\Lambda = \Lambda(\mathrm{brems}) + \Lambda_c$. We assume $\Lambda = 0$ for $T < 10^3$ K, because we are interested only in the region hotter than 10^6 K, and not in the cooled dense shell. The ambient gas is fixed as $n_0 = 1$ atom cm^{-3} and $T = 10^3$ K. Except for the models in section 5, the data for the supernova explosion and ambient matter are fixed as the above.

As a reference for the X-ray line emission, the volume emissivity of O VII (0.57 keV) line is calculated by the simple algebraic formula:

$$\Lambda(\mathrm{O\ VII}) = 9.77\times10^{-25} n^2 \exp\left[-16.7(\log T - 6.3)^2\right]\,, \tag{2.9}$$

which is an interpolation of the results by Kato (1976). The ionization equilibrium assumed in equation (2.9) does not generally hold in the SNR shell. We use this equation only to indicate the line emission region.

2.3. *Numerical Test: An Isolated SNR*

Using the above data, the expansion of an isolated SNR in a uniform medium is simulated in order to test the numerical code and to construct the standard SNR model in this paper.

A test of the numerical code is performed on the following two points: Firstly, the expansion of an SNR shell satisfies the similarity law, $R_s \propto t^{0.4}$ in the adiabatic phase and the isomomentum law, $R_s \propto t^{0.25}$ in the radiative phase, R_s being the radius of shock front. Secondly, the density distribution reproduces the Sedov solution in the adiabatic phase (Sedov 1959).

In figure 1, the expansion law of the shock front is shown. The transition from the adiabatic phase to the radiative phase occurs at $\sim 2.0\times10^{12}$ s. The shell destruction time, at which the pressure at the shock front becomes equal to the pressure in the ambient matter, is about 6×10^{13} s. The density distributions at various stages are illustrated in figure 2. Since the radiative cooling for $T < 10^3$ K is omitted, the shell compression is rather small.

The calculated results of the density distribution were compared with those of Sedov's (1959) solution. Except for the neighborhood of the shock front, where the density jump is artificially smoothed out, the results are in good agreement with Sedov's (1959) results.

When compared with numerical results by Chevalier (1974), Mansfield and Salpeter (1974), and Straka (1974), the general trends are in good agreement with theirs. There are, however, some differences among these results, when examined closely. They are the transition time from the adiabatic to the radiative phase, the expansion law at the radiative phase, and the structure of the shocked region. These differences are mainly due to the differences in the cooling rates adopted and to the treatments of shock discontinuity. The present calculations by means of rather large Eulerian meshes have shortcomings in the reproduction of a highly compressed shell, because the shocked region becomes averaged over two- or three-meshes of large size. As far as the dynamics of two interacting

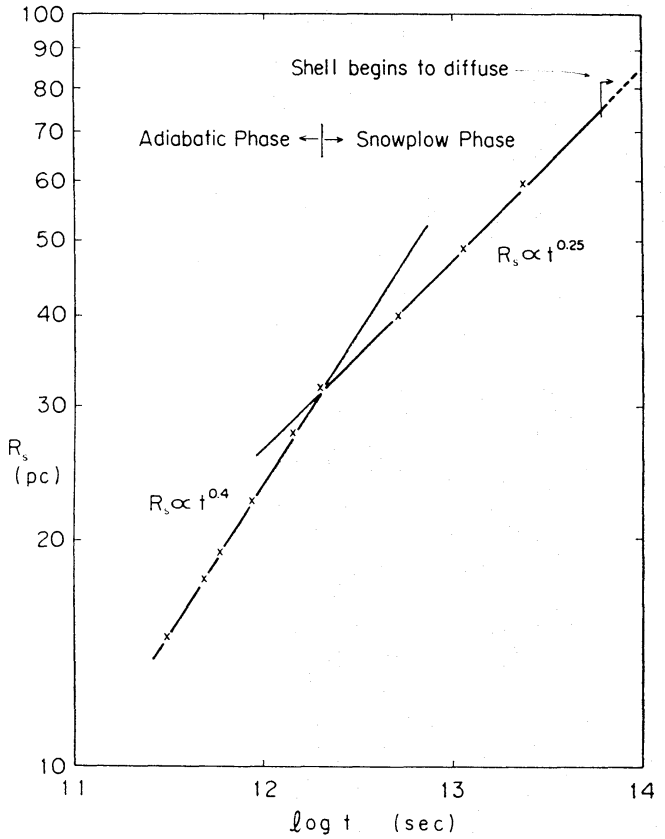

Fig. 1. Time variation of the radius of shock front in the case of a point explosion in a uniform medium.

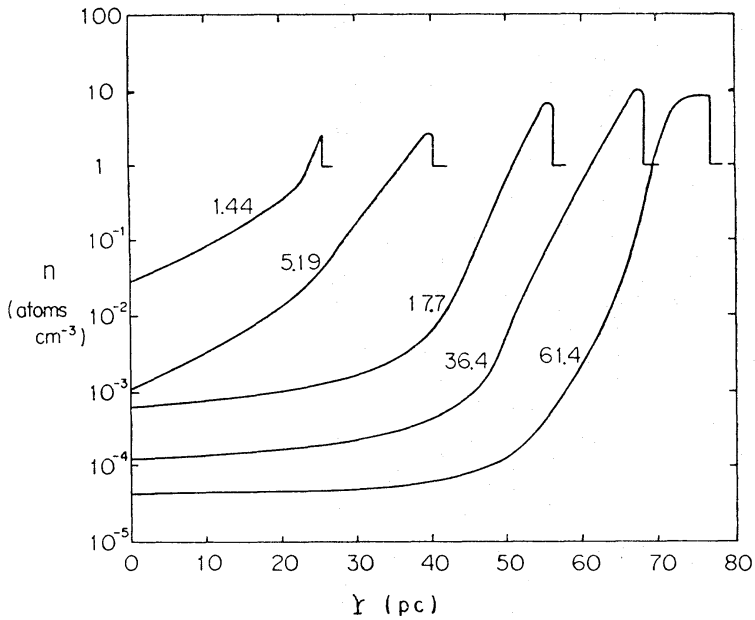

Fig. 2. Density distributions plotted against radial distance r for the cases of an isolated SNR. Curves are labeled with the value of the age in units of 10^{12} s.

Table 1. Summary of the calculated models when the second explosion is outside the first one.

Model No.	t_0 (s)	D (pc)	t_E (s)	$R_s^{(1)}(t_E)$ (pc)	Comments
Model I	1×10^{12}	40	1.23×10^{12}	26.5	M-S, figure 3
Model II	3×10^{11}	40	7.75×10^{11}	22.0	M-S, not illustrated
Model III	3×10^{12}	40	3.02×10^{12}	35.4	M-S, figure 4
Model IV	3×10^{13}	80	3.04×10^{13}	63.6	M-AS, figure 5
Model V	1×10^{13}	120	2.95×10^{13}	63.2	NM, figure 6

The meanings of t_E, M-S, M-AS, and NM are described in the tevt.

SNRs is concerned, the detailed structure of a compressed shell is of little importance.

3. *Second Supernova Explosion outside the First SNR Shell*

In this section, we study interacting SNRs such that the second supernova explosion occurs at the time t_0 after the first supernova explosion at the distance D from the first explosion point and outside the first SNR shell. The time of this system is measured from the time of the first explosion. The radii of the first and second SNRs are designated as $R_s^{(1)}(t)$ and $R_s^{(2)}(t)$, respectively. Then, $R_s^{(1)}(t_0)<D$ holds. In table 1, the parameters of the calculated models are summarized, where the encounter time t_E of two-SNR shells, which is given by $R_s^{(1)}(t_E)+R_s^{(2)}(t_E-t_0)=D$, and $R_s^{(1)}(t_E)$ are also given.

3.1. *Evolution of Two Interacting SNRs: Model I*

As is seen in table 1, both SNRs at the encounter time are in the adiabatic phase. Just after the encounter of the SNR shells, the collided-shell edges are highly compressed due to the overlapping of two dense fronts. At the same time, the dissipation of kinetic energies of the expanding shells increases the pressure as well as the temperature, and this compressed edge expands in the plane perpendicular to the line connecting two-SNR centers. As is seen from figures 3a and 3b, the expanding shell becomes peanut-shape as a whole. The density in the adjoining shell is 3–4 times larger than that in the other shell region. Then, the adjoining shell edge is first cooled. This edge will look like a ring connecting two SNRs.

In the SNR cavity, the matter flow from the younger SNR 2 overcomes that from the older SNR 1, and then the cavity of SNR 1 is filled by the matter flowing in from SNR 2. When the expanding front of SNR 2 takes over the shell across the cavity of SNR 1, the cavity of SNR 1 becomes an almost isodensity state as in figure 3c. As is seen in figures 3d and 3e, the SNR structure becomes nearly symmetric with respect to each other and the later evolution becomes rather simple. The common cavity of two SNRs shows a pattern of density distribution as if the matter flow arises at the center of SNR 2. The expanding dense shell is cooled and compressed.

At the final stage in this computation, the radii of two SNRs measured along the Z-axis are nearly equal to each other, $\sim$68 pc, which is about 1.05 times the isolated one of the same age. At this stage, the volume occupied by two interacting SNRs is about 0.86 times those of two isolated SNRs. After all, the differences of evolutionary stages of two SNRs at the encounter time are almost erased

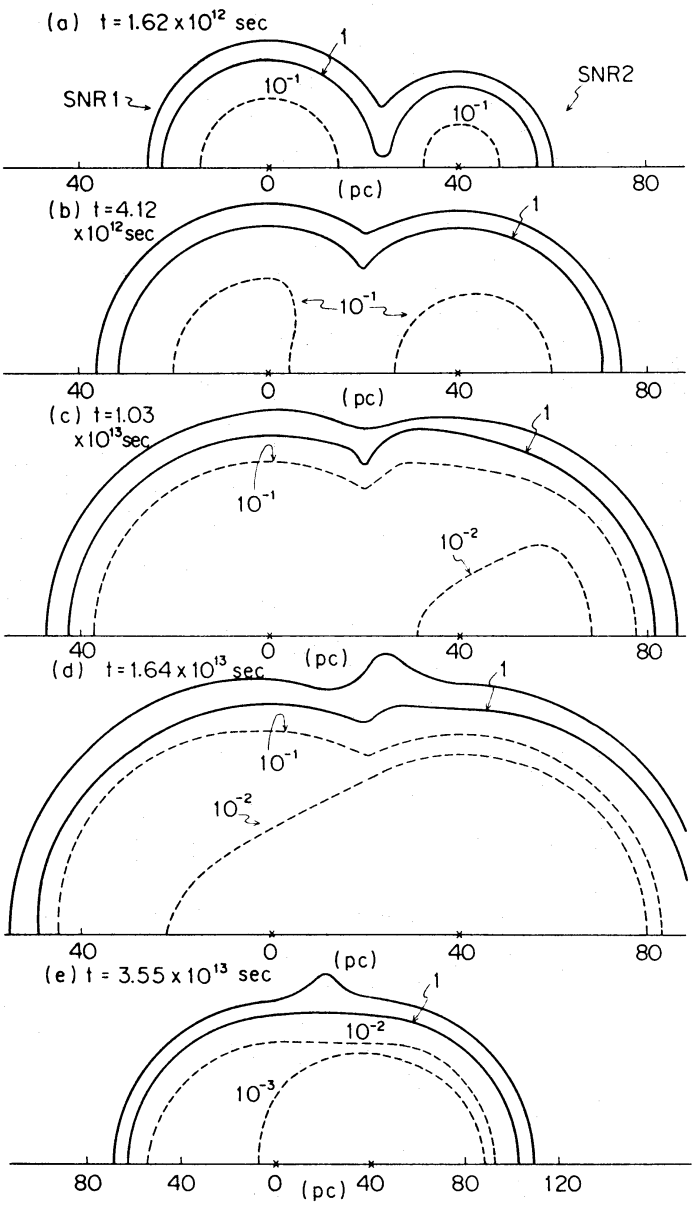

Fig. 3. Density profiles of interacting SNRs at the typical five stages in the case of Model I. The outermost solid line shows the most dense shell and the inner solid line is for $n=1$ atom cm^{-3}. Then, the region surrounded by these two solid lines is the compressed shell by the shock wave. Two crosses show the explosion points. Contours are labeled with the value of number density in atoms cm^{-3}.

at the final stage, and two SNRs merge into a single-like SNR.

3.2. *Evolutionary Features of Other Models*

Here, the models of different t_0 and D are studied in order to see the results in the cases of different evolutionary stages of two SNRs at the encounter time.

First, by fixing the distance D the same as in Model I, we vary the time of the second explosion. As easily inferred, the structure of Model II becomes more symmetric with respect to two SNRs than that of Model I. The matter flow in

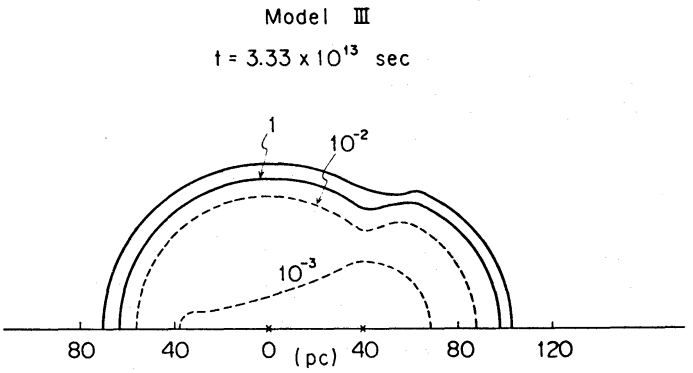

Fig. 4. Density profiles in the case of Model III at the final stage in the present computations.

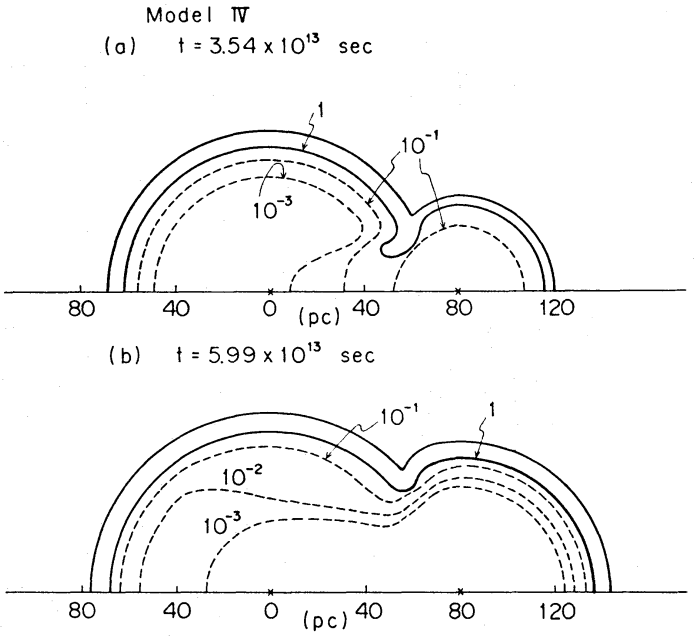

Fig. 5. Density profiles in the case of Model IV at the two typical stages.

the cavity roughly resembles that for an explosion at the middle point of two-SNR centers. In the case of Model III, SNR 1 is in the early radiative phase at the encounter time and the second explosion occurs just outside the cooled shell of SNR 1. Although the adjoining edge is compressed to produce a highly dense shell, the cooling efficiency is so much smaller than the dissipational heating that the pressure increases to make a hole. This hole becomes large as time goes on due to the rapid expansion of SNR 2, and two SNRs merge into a single-like SNR as in figure 4.

As the second case, Model IV with D=80 pc and $t_0=3\times10^{13}$ s is studied. The structures of two stages are shown in figures 5a and 5b.

At the stage (a), a small hole is opened in the adjoining edge and the hot matter of SNR 2 begins to flow into the cavity of SNR 1. As a result of this matter flow, the density of the SNR 1 cavity becomes larger at the stage (b) than that at the stage (a). Although the pressure of this invading hot matter works as a piston to the SNR 1 shell, this does not much affect the expansion

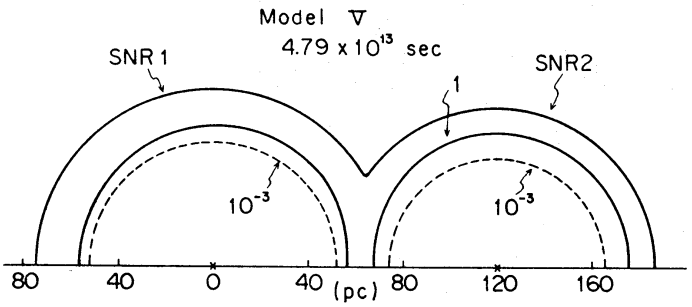

Fig. 6. Density profiles in the case of Model V. This is a representative of the non-merged case.

law of SNR 1. Thus, the lifetime of SNR 1 is prolonged only by a factor of 1.05 compared with the one of an isolated SNR. On the other hand, as to SNR 2, the encounter effect does not appear in the right half. That is, the energy and momentum of SNR 2 only in the region overlapped with SNR 1 are used to rejuvenate SNR 1.

As the third case, we study Model V, in which both SNRs at the encounter time are in the late radiative phases. In figure 6, a typical structure is illustrated. In this case, the matter at the adjoining edge is highly compressed and, at the same time, is rapidly cooled, so that the pressure at the edge does not increase but rather decreases. Thus, the wall of an adjoining edge becomes denser so that two SNRs do not merge. Except for the dense wall, both SNRs evolve as independent SNRs.

3.3. *Summary of Results*

Inspection of the calculated results in the above reveals that the SNR collision from outside of the first SNR shell can be classified into two typical cases: (M) the merged case and (NM) the non-merged case. The former case may also be divided into two cases, i.e., (M-S) the symmetrical and single-like SNR formation as Models I–III and (M-AS) the asymmetrical and peanut-shape SNR formation as Model IV. These classifications are denoted in the final column in table 1.

The differences between the merged case and non-merged case will be understood through the following discussion. We consider that the adjoining edge is formed after the encounter, and its density and temperature reach $\bar{\rho}$ and $\bar{T}$. Then, the cooling rate in this shell is $\Lambda(\bar{\rho}, \bar{T})$, while the heating rate by the dissipation of kinetic energies of two colliding shells is, at most, $\Gamma=(\rho_1 v_1^2/\tau_1+\rho_2 v_2^2/\tau_2)/2$. Here, ρ_i and v_i $(i=1, 2)$ are the densities and velocities of two colliding shells, and τ_i the dissipation times of kinetic energies, are

$$\tau_i=R_s^{(i)}/v_i \qquad (i=1, 2) .$$

In the merged case, $\Gamma>\Lambda$ holds. Especially, in Models I–III $\Gamma\gg\Lambda$ holds. In the non-merged case, $\Lambda>\Gamma$ holds already at the encounter time. Thus, the adjoining edge is cooled more and more as the encounter proceeds.

The classification into the merged and non-merged cases may be done in terms of one parameter D. From the above results, the critical distance $D_{\rm crit}$ which distinguishes two cases from each other is estimated as $D_{\rm crit}\simeq 100$ pc. When $D>D_{\rm crit}$, both SNRs are in the radiative phase at the encounter time and $\Lambda>\Gamma$ holds irrespective of t_0. On the other hand, the merger of two SNRs takes place when $D<D_{\rm crit}$. Within the present computations, the upper limit of D for

two SNRs to merge into a single-like SNR is estimated to be ~50 pc.

4. *Second Explosion inside the First SNR Shell*

In this section, we study the case in which the second supernova explosion occurs in the cavity of the first SNR (SNR 1), and the expanding front of the second SNR (SNR 2) takes over the SNR 1 shell.

In table 2, the age t_0 and the radius $R_s^{(1)}(t_0)$ of SNR 1 at the time of second explosion, and the distance D between two-explosion points studied in the present calculation are summarized.

4.1. *Second Explosion in the SNR Cavity: Models VI, VII,* and *VIII*

In figure 7, the structures of interacting SNRs in the case of Model VI are

Table 2. Summary of the calculated models when the second explosion is in the cavity.

Model No.	t_0 (s)	D (pc)	$R_s^{(1)}(t_0)$ (pc)	α	Comments
Model VI	3×10^{13}	40	63.4	1.81	S, figure 7
Model VII	3×10^{13}	20	63.4	1.89	S, not illustrated
Model VIII	3×10^{13}	56	63.4	1.41	B, figure 8
Model IX	6×10^{12}	40	42.4	1.42	B, not illustrated
Model X	3×10^{12}	20	35.6	1.90	S, not illustrated

The parameter α and the meanings of S and B are described in the text.

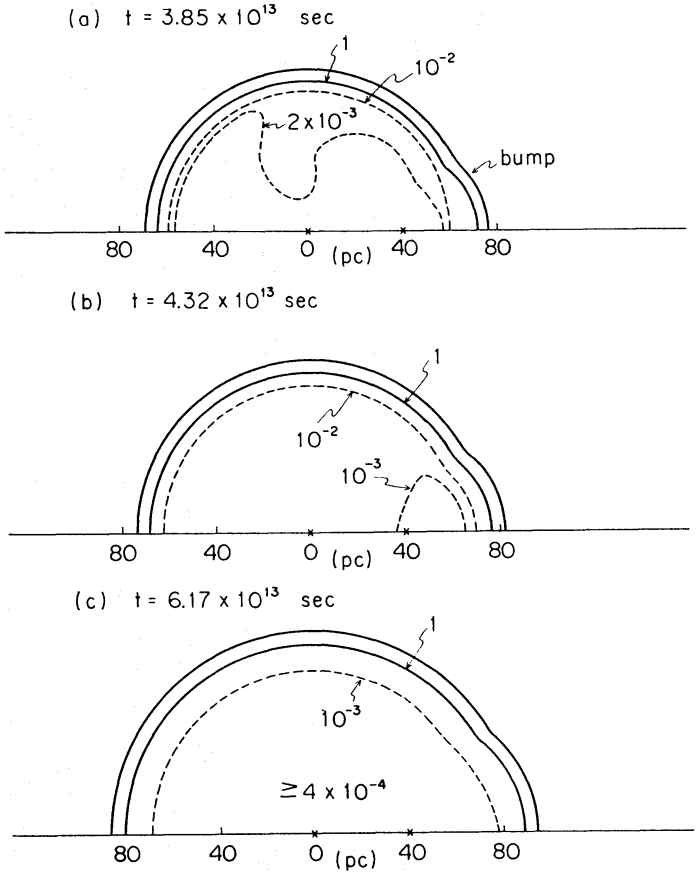

Fig. 7. Density profiles in the case of Model VI at the three typical stages.

shown for three typical stages. Within 10^{13} s after the second explosion, the flow from SNR 2 to the center of SNR 1 is impeded by the expanding matter flow from the SNR 1 center. Thus, the density hump is formed in the SNR 1 cavity due to the collision of two matter flows as in figure 7a. This hump moves to the SNR 1 shell. On the other hand, in the direction opposite to the center of SNR 1 the expanding front takes over the SNR 1 shell immediately and pushes outwards.

After the time of 10^{13} s, the shock front of SNR 2 takes over the SNR 1 shell in all directions. At this time, the SNR 1 shell is pushed as a whole and is adiabatically compressed, so that the expansion is accelerated till the radiative cooling overweighes again. Especially, the shell edge near the SNR 2 center receives much momentum and grows as a bump.

Shortly thereafter, as in figure 7c, the matter motions inside the cavity are made even and the density distribution becomes smoother than that of an isolated SNR. Even in this stage, the pressure of the expanding shell is about twice that of the ambient matter, and the expansion proceeds further. The average radius of SNR 1 in the stage of figure 7c is about 86 pc, which is larger by a factor of 1.16 than that of an isolated SNR of the same age. Due to the overtaking of the SNR 2 shell, the total momentum of the SNR 1 shell is multiplied by a factor of 1.81. This multiplication factor is denoted as α in table 2.

After this stage, the SNR shell expands for 7.3×10^{13} s and begins to diffuse. A small bump formed by the impact of SNR 2 becomes inconspicuous because the final radius attains to be about 90 pc. Then, this SNR appears to be an isolated one as a whole.

As is easily supposed, the case of Model VII, in which the distance between two explosion points is smaller than that in Model VI, show a single-like structure in an early stage as for the degree of the sphericity of the dense shell and the density distribution in the cavity. The expansion law is not much altered from that of Model VI.

In Model VIII, the case of the second explosion just inside the expanding shell of SNR 1 is studied. In this model, the wall of the dense shell stands close to the SNR 2 center and a comparatively large part of explosion energy works as a piston to the wall. Thus, the preceding shell is pushed and blown up as in figure 8a. On the other hand, a density hump is formed in the SNR 1 cavity. Subsequently the common cavity becomes an isodensity state as in figure 8b similar to the two above models. The bump formed by the impact of SNR 2 expands like an SNR fragment. The stagnation point appears at the overlapped region of two shells. The average radius of the front of SNR 1 at the stage (b) is about 1.09 times as large as an isolated one, and that of SNR 2 at the spherically expanding part is about 0.94 times. The total lifetime of SNR 1 is prolonged to $\sim6.7\times10^{13}$ s and that of SNR 2 is shortened to $\sim5.5\times10^{13}$ s.

4.2. *Summary*

In the case of Model IX, the second explosion occurs just inside of the SNR 1 shell, which is similar to Model VIII. The final structure and the expansion law are nearly equal to those of Model VIII, but the bump formed by the second explosion is not so conspicuous because the difference in the ages of two SNRs is small. In the case of Model X, two SNRs evolve as almost a single-like SNR exploding at the middle point of the two SNR centers. This resembles Model VII.

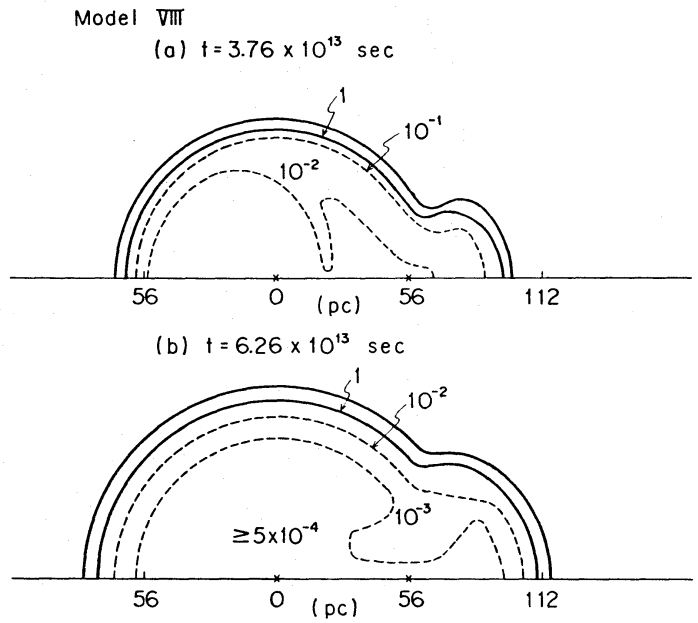

Fig. 8. Density profiles in the case of Model VIII at the two typical stages.

Summarizing the above results, the final SNR structures can be classified into the following two types. Type S: the second explosion has little influence on the spherical shape of the first expanding shell, and the resultant SNR structure resembles an isolated one. Type B: due to the strong impact of the second explosion the bump is formed at the shell edge close to the center of SNR 2. The preceding SNR is rejuvenated, and the bump expands as a short-lived remnant of the second explosion.

The critical distance, $D_{\rm crit}$, for the above classification is estimated as follows: Firstly, we consider the encounter time $t_{\rm E}$, when the radius of the shock front of SNR 2 extends to $R_{\rm s}^{(2)}(t_{\rm E}-t_0)=[R_{\rm s}^{(1)}(t_{\rm E})^2-D_{\rm crit}^2]^{1/2}$. At this time, a half of the energy of SNR 2, at least, reaches the SNR 1 shell and works as a piston to the shell. Then, we compare it with the energy of SNR 1 within this front. If $D_{\rm crit}$ is so small, these two are comparable to each other and the spherical shape of the SNR 1 shell is conserved. However, if $D_{\rm crit}$ is as large as $R_{\rm s}^{(1)}(t_{\rm E})$, the energy brought about by SNR 2 overweighs that of SNR 1, and a highly reheated shell expands rapidly.

It is generally difficult to determine the numerical values of $D_{\rm crit}$, because this depends sensitively upon the evolutionary stage of SNR 1. Roughly speaking, a single-like SNR is formed when $D\leq D_{\rm crit}\simeq 2R_{\rm s}^{(1)}(t_0)/3$, and in this case the total acquired momentum is larger by a factor of 1.6–1.9 than that of an isolated SNR.

5. *X-Ray Profiles of Two Interacting SNRs*

From the observations of soft X-ray background below 2 keV, the solar neighborhood is presumed to be within a local hot bubble of $n\sim 10^{-2}$ atoms cm^{-3} and $T\sim 10^6$ K. This hot region overlaps with the hot region of loop I. The fact that loop I is a hunge SNR is confirmed by the discoveries of a shell structure in X-ray observations (Cruddace et al. 1976; Hayakawa et al. 1977; Borken and Iwan 1977). Then, provided that the hot bubble in the solar neighborhood is an

old SNR, the encounter of these two SNRs may be expected (Tanaka and Bleeker 1977; Hayakawa et al. 1978). Moreover, the encounter of loop I and loop IV SNRs is suggested by Borken and Iwan (1977).

Then, in this section the X-ray profiles of two interacting SNRs are calculated. The distance between two SNR centers is fixed to be 150 pc, and two cases of the ambient gas density are examined for $n_0=10^{-1}$ and 10^{-2} cm^{-3}.

In table 3, three calculated models are summarized. Models A and B correspond to the case of the second explosion outside the SNR 1 shell, and Model C to the case of that inside the SNR 1 shell. In figures 9, 10, and 11, the density profiles and the contours of volume emissivities of 0.1-keV thermal bremsstrahlung and O VII (0.57 keV) line emission are illustrated for the respective models. The selected stages nearly correspond to those when the X-ray counts from SNR2 are about the same as those from loop I.

In the cases of Models A and B, a highly dense and cooled shell is formed at the adjoining edge. In the contour of soft X-ray emission, this edge appears as a local minimum as if there is a dense cloud absorbing the soft X-rays. Although 0.1 keV and O VII line emissions are stronger just inside the adjoining edge, the emission region in Model B does not show a shell structure. This is because the gas density in the cavity is so small. In figure 9, the X-ray emitting region shows a shell structure although it is distorted. The cooled shell emitting the radio continuum looks like a shell, but this dense shell does not continue till it reaches the plane. In figure 9, the directions of maximum compression at the dense shell are also shown by the arrows.

In the case of Model C as in figure 11, the shock wave of the second explosion rapidly sweeps the cavity, so that the X-ray emitting shell is not formed between two SNRs, but two SNRs are within a huge hot bubble.

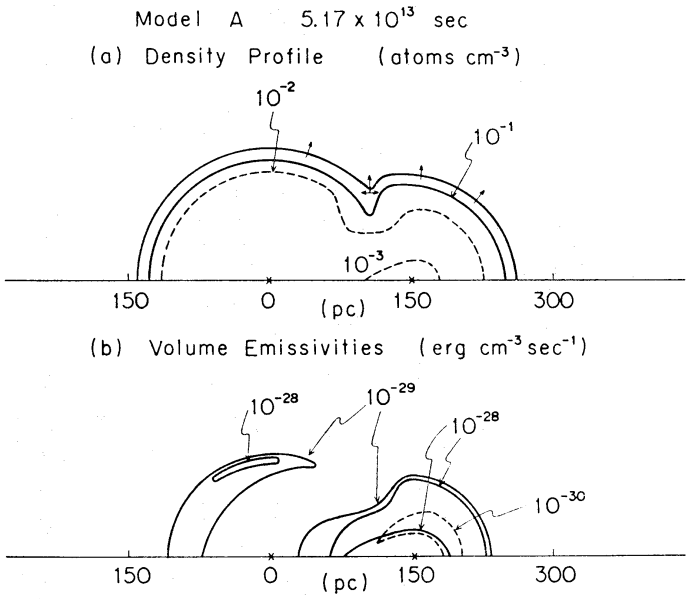

Fig. 9. (a) Density profiles in the case of Model A. A highly compressed and cooled region appears at the boundary of two SNR shells. The arrows show the directions of the maximum compression. (b) Contours of volume emissivities in 0.1-keV thermal bremsstrahlung (solid lines) and O VII (0.57 keV) line emissions (dashed line). A distorted shell structure is observed between two SNRs.

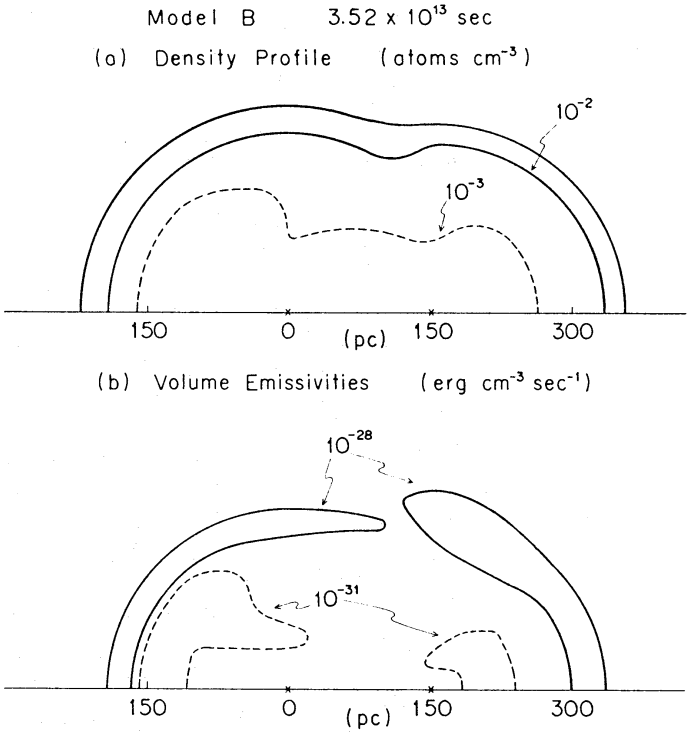

Fig. 10. The same as in figure 9 but in the case of Model B.

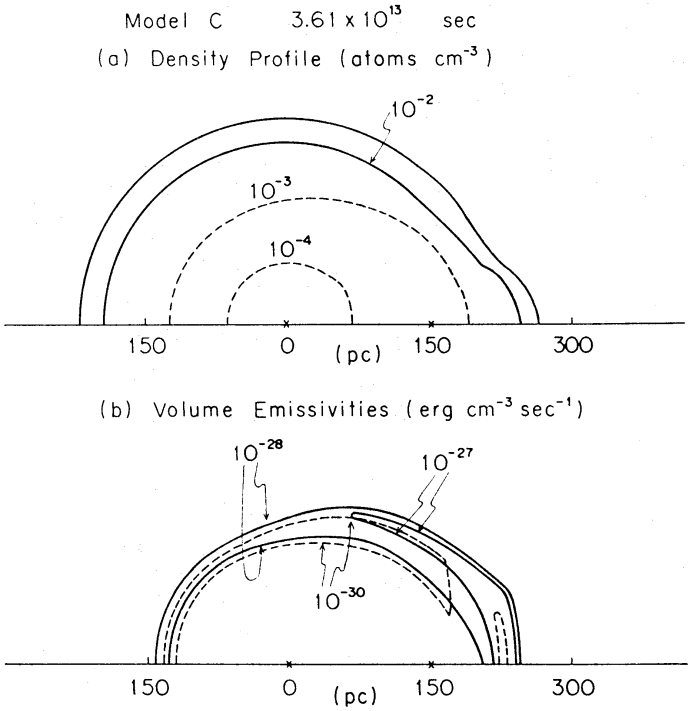

Fig. 11. The same as in figure 9 but in the case of Model C. The second explosion within the cavity of SNR 1 results in a single-like SNR.

Table 3. Summary of the calculated models of two interacting SNRs.

Model name	n_0 (cm^{-3})	D(pc)	t_0 (s)	Comments
Model A	10^{-1}	150	3×10^{13}	figure 9
Model B	10^{-2}	150	1×10^{13}	figure 10
Model C	10^{-2}	150	3×10^{13}	figure 11

6. *Discussion*

Summarizing the results in subsections 3.3 and 4.2, the structural changes of interacting SNRs are arranged in terms of one parameter D. Namely, if Types S and B in section 4 are regarded to be the same types as (M-S) and (M-AS) in section 3, respectively, the final structures of two interacting SMRs can be classified into three types: (1) two SNRs merge into a single-like SNR, when $D\leq D_{\rm crit}(1)\simeq$(40–50) pc, (2) they merge but show a peanut-shape structure, when $D_{\rm crit}(1)\leq D\leq D_{\rm crit}(2)\simeq100$ pc, and (3) they are almost independent except for the adjoining edge, when $D_{\rm crit}(2)\leq D\leq160$ pc.

From the theoretical point of view, two interesting problems are indicated in relation to the interacting SNRs. One is the formation of the SNR tunnel systems in our Galaxy, and the other is the gas ejection from a galaxy driven by a burst of supernova explosions.

The former is first proposed by Cox and Smith (1974) in relation to the observations of the soft X-ray background. When the supernova rate is $r_{\rm SN}$ per galaxy, the volume of an isolated SNR at its death is $V_{\rm SNR}$, and its age is $\tau_{\rm SNR}$, the porosity is given as

$$q=r_{\rm SN}\tau_{\rm SNR}V_{\rm SNR}/V_{\rm G}\ , \tag{6.1}$$

where $V_{\rm G}$ is the volume of a galaxy and all SNRs are assumed to be isolated. The fraction of the volume occupied by SNRs becomes $f=1-\exp(-q)$ when $q\ll1$. Then, the probability for another supernova explosion to occur at the distance D from the SNR of the nearest neighbor is given as

$$f_D=1-\exp[-q(D/R_{\rm SNR})^3]\ , \tag{6.2}$$

where $R_{\rm SNR}$ is the final radius of an SNR, i.e., $R_{\rm SNR}=(3V_{\rm SNR}/4\pi)^{1/3}$.

In terms of two critical distances of $D_{\rm crit}(1)$ and $D_{\rm crit}(2)$ in the above, we can estimate the probabilities of merging into a single-like SNR and to a peanut-shape one, respectively, as

$$f_{\rm s}=1-\exp\{-q[D_{\rm crit}(1)/R_{\rm SNR}]^3\}\simeq0.05 \tag{6.3}$$

and

$$f_{\rm p}=1-f_{\rm s}-\exp\{-q[D_{\rm crit}(2)/R_{\rm SNR}]^3\}\simeq0.28\ , \tag{6.4}$$

where we have taken the values of parameters as $D_{\rm crit}(1)=50$ pc, $D_{\rm crit}(2)=100$ pc, $r_{\rm SN}=0.01$ SN yr^{-1}, $\tau_{\rm SNR}=6\times10^{13}$ s, $R_{\rm SNR}=75$ pc, and $V_{\rm G}=\pi(15\ {\rm kpc})^2(300\ {\rm pc})\simeq2\times10^{11}$ $\simeq$pc^3. (In this case, q becomes ~0.17 and $f\simeq q$.) From equations (6.3) and (6.4), we estimate that within the radius of 1.5 kpc from the Sun, there may be 3–4 SNRs, which are younger than 10^5 yr and show some characteristics of the SNR

collision. Moreover, there are about 100 SNRs with ages as old as 10^6 yr within the same region. In these SNRs, about 28 SNRs will be rejuvenated and about 5 SNRs will look like a huge SNR even if the ambient gas density is as high as 1 atom cm^{-3}. From these, we may conjecture that the O VI absorptions originate in the rejuvenated SNRs and the soft X-ray emissions in the younger SNRs.

As for the latter problems, the following situations will be expected. From the studies of the chemical evolution of a galaxy (Larson 1974; Tinsley 1977), the supernova events in an early stage ($\lesssim 10^9$ yr) of a galaxy occur as frequently as 1–10 SN yr^{-1}, so that the porosity q becomes larger than unity. Thus, the SNR collisions successively occur and all SNRs merge into one SNR. Finally, the whole volume of a galaxy will be filled with SNRs (Schwarz et al. 1975; Takahara and Ikeuchi 1977; Ikeuchi 1977).

Here, we will examine the condition for the interstellar gas to be swept out to the outside of a galaxy. At first, we simply assume that, if the succeeding explosion occurs within $D \lesssim D_{\rm crit}(1)$ and $t \lesssim t_{\rm c}$, the interacting SNRs merge into a single SNR. From this assumption, if the mean distance $\bar{D}$ of SNRs younger than $t_{\rm c}$,

$$\bar{D}=(3V_{\rm G}/4\pi r_{\rm SN} t_{\rm c})^{1/3} \simeq 27\left[\frac{V_{\rm G}}{2\times 10^{11}({\rm pc})^3}\frac{10^6{\rm yr}}{t_{\rm c}}\frac{10\ {\rm SN\ yr^{-1}}}{r_{\rm SN}}\right]^{1/3}, \tag{6.5}$$

is smaller than $D_{\rm crit}(1)$, all SNRs will merge into a huge single SNR. In this case, the porosity is already greater than unity, and as a whole the galaxy becomes a SNR cavity. From equation (6.5), this condition is satisfied if $t_{\rm c}=10^6$ yr and $r_{\rm SN} \gtrsim 2$. Thus, the gas sweeping in an early explosive era of a galaxy is expected.

Of course, the above discussions are too crude. It is necessary to study this problem quantitatively in the same manner as Smith (1977), also including the gas motion. At least, we can say that once a huge SNR has been formed, this will grow increasingly due to the feeding of new SNRs.

References

Borken, R. J., and Iwan, D. C. 1977, *Astrophys. J.*, **218**, 511.

Burstein, P., Borken, R. J., Kraushaar, W. L., and Sanders, W. T. 1977, *Astrophys. J.*, **213**, 405.

Castor, J., McCray, R., and Weaver, R. 1975, *Astrophys. J. Letters*, **200**, L107.

Chevalier, R. A. 1974, *Astrophys. J.*, **188**, 501.

Cox, D. P., and Smith, B. W. 1974, *Astrophys. J. Letters.*, **189**, L105.

Cox, D. P., and Tucker, W. H. 1969, *Astrophys. J.*, **157**, 1157.

Cruddace, R., Friedman, H., Fritz, G., and Shulman, S. 1976, *Astrophys. J.*, **207**, 888.

Hayakawa, S., Kato, T., Nagase, F., Yamashita, K., Murakami, T., and Tanaka, Y. 1977, *Astrophys. J. Letters*, **213**, L109.

Hayakawa, S., Kato, T., Nagase, F., Yamashita, K., and Tanaka, Y. 1978, *Astron. Astrophys.*, **62**, 21.

Hayakawa, S., Kato, T., Tanaka, Y., Yamashita, K., Bleeker, J. A. M., and Deerenberg, A. J. M. 1975, *Astrophys. J.*, **195**, 535.

Ikeuchi, S. 1977, *Prog. Theor. Phys., Kyoto*, **58**, 1742.

Itoh, H. 1977, *Publ. Astron. Soc. Japan*, **29**, 813.

Kato, T. 1976, *Astrophys. J. Suppl.*, **30**, 397.

Larson, R. B. 1974, *Monthly Notices Roy. Astron. Soc.*, **169**, 229.

Lax, P. D. 1954, *Commun. Pure Appl. Math.*, **7**, 159.
Lax, P. D., and Wendroff, B. 1966, *Commum. Pure Appl. Math.*, **13**, 217.
Mansfield, V. N., and Salpeter, E. E. 1974, *Astrophys. J.*, **190**, 305.
Naranan, S., Shulman, S., Friedman, H., and Fritz, G. 1976, *Astrophys. J.*, **208**, 718.
Schwarz, J., Ostriker, J. P., and Yahil, A. 1975, *Astrophys. J.*, **202**, 1.
Sedov, L. I. 1959, *Similarity and Dimensional Methods in Mechanics*, ed. M. Holt, translated by M. Friedman (Infosearch Ltd., London), p. 146.
Smith, B. W. 1977, *Astrophys. J.*, **211**, 404.
Spitzer, L., and Jenkins, E. B. 1975, *Ann. Rev. Astron. Astrophys.*, **13**, 133.
Straka, W. C. 1974, *Astrophys. J.*, **190**, 59.
Takahara, F., and Ikeuchi, S. 1977, *Prog. Theor. Phys., Kyoto*, **58**, 1728.
Tanaka, Y., and Bleeker, J. A. M. 1977, *Space Sci. Rev.*, **20**, 815.
Tinsley, B. M. 1977, *Astrophys. J.*, **211**, 621.
Woltjer, L. 1972, *Ann. Rev. Astron. Astrophys.*, **10**, 129.